2022

Localization effects and Anomalous Hall conductivity in a disordered 3D ferromagnet

Paul M. Shand

Y. Moua

G. Baker

Shah R. Valloppilly

Pavel V. Lukashev

See next page for additional authors

Authors
Paul M. Shand, Y. Moua, G. Baker, Shah R. Valloppilly, Pavel V. Lukashev, and Parashu Kharel

Localization effects and Anomalous Hall conductivity in a disordered 3D ferromagnet

P. M. Shand,[1*] Y. Moua,[1] G. Baker,[2] S. Valloppilly,[3] P. V. Lukashev,[1] and P. Kharel[2]

[1]*Department of Physics, University of Northern Iowa, Cedar Falls, IA 50614-0150, USA*

[2]*Department of Physics, South Dakota State University, Brookings, South Dakota 57007, USA*

[3] *Nebraska Center for Materials and Nanoscience, University of Nebraska, Lincoln, NE 68588, USA*

*paul.shand@uni.edu (corresponding author)

Abstract

We have prepared the Heusler alloy $CoFeV_{0.5}Mn_{0.5}Si$ in bulk form via arc melting. $CoFeV_{0.5}Mn_{0.5}Si$ is ferromagnetic with a Curie temperature of 657 K. The longitudinal resistivity exhibits a minimum at 150 K, which is attributable to competition between quantum interference corrections at low temperatures and inelastic scattering at higher temperatures. The magnetoresistance (MR) is positive and nearly linear at low temperatures and becomes negative at temperatures close to room temperature. The positive MR in the quantum correction regime is evidence of the presence of the enhanced electron interaction as a contributor to the longitudinal resistivity. Hall effect measurements indicate a carrier concentration of the order of 10^{22} cm^{-3}, which is nearly 3 orders of magnitude higher than that found in the "parent" material CoFeMnSi. The higher carrier concentration is consistent with the predicted half metallicity of $CoFeV_{0.5}Mn_{0.5}Si$. The anomalous Hall conductivity of $CoFeV_{0.5}Mn_{0.5}Si$ is temperature independent for temperatures below the resistivity minimum, which is strong evidence of the absence of quantum interference effects on the anomalous Hall conductivity in a 3D ferromagnet.

Keywords

Half metals, magnetically ordered materials, transition metal alloys and compounds, electrical transport, electron-electron interactions.

Published (2022) in Journal of Magnetism and Magnetic Materials, 563, art. no. 170035, .
DOI: 10.1016/j.jmmm.2022.170035

1. Introduction

The research literature on Heusler alloys is voluminous and varied. The innumerable combinations of structural and atomic constituents makes for a rich and interesting variety of physical and chemical properties that continue to be explored [1–6]. Much of the most recent research on Heusler alloys has dealt with the existence of half-metallicity and concomitant spin-polarized transport at room temperature and above [7–11]. These findings have generated a great deal of excitement in view of the potential for applications in the still budding field of spintronics [12–15].

The band structure is key to understanding and exploiting the electronic and magnetic properties of these Heusler alloys. Half metallicity and spin gapless semiconductor behavior are due to the existence of a band gap in one of the two spin channels. In half metals, the Fermi level lies within this gap but traverses bands of the opposite spin within the Brillouin zone. In spin gapless semiconductors, the Fermi-level traversal is at a zero-gap coincidence in one of the two spin bands [16–19]. The band structure – specifically, hybridization of transition-metal *d* states and of the *sp*-atom states – also leads to magnetic properties such as Slater-Pauling behavior of the magnetic moment per formula unit[20–22].

Extrinsic factors also play an important role in the transport and magnetotransport properties of Heusler alloys. As-prepared alloys often exhibit disorder among the atoms in different sublattices [2,23,24]. Such disorder, along with other inhomogeneities (defects, impurities, grain boundaries, etc.), can lead to a negative temperature coefficient of resistance over a wide temperature range due to elastic scattering. In some cases, a resistivity minimum occurs, typically below room temperature [25–27]. The resistivity minimum occurs because of a competition between inelastic scattering processes that dominate at high temperatures and carrier-localization mechanisms — in particular, weak localization and the enhanced electron interaction — that prevail at low temperatures [28].

The Hall effect is also influenced by both band structure and extrinsic factors. In particular, the anomalous Hall effect derives from the effect of the spin-orbit interaction on band structure (intrinsic) or scattering of carriers (extrinsic). The band-structure contribution can be explained in terms of the Berry curvature [29–33]. Extrinsic effects include skew scattering and the side-jump mechanism [34]. The relative size of these contributions depends on the longitudinal resistivity.

Recent work by Hazra *et al* [27,35] has examined the interplay between localization effects and the various contributions to the anomalous Hall effect in thin films of Co_2FeSi. They found that the longitudinal resistivity correction due to the enhanced electron interaction vanishes for the anomalous Hall resistivity, as predicted by theory for two-dimensional systems [36–38]. Hazra *et al* also found a low value of the zero-magnetic field anomalous Hall conductivity relative to many other ferromagnets, which was ascribed to the absence of band-structure resonances that boost the intrinsic contribution to the anomalous Hall conductivity. Similar work on the connection between localization and the anomalous Hall effect in ferromagnetic $Ga_{1-x}Mn_xAs$ epilayers was carried out by Mitra et *al* [39]. Bainsla *et al* investigated the anomalous Hall effect in CoFeMnSi to shed light on the spin gapless semiconducting behavior of this material [40]. A comparatively small value of the anomalous Hall conductivity was found in this material as well, though there was no minimum in the longitudinal resistivity in the investigated temperature range between 5 K and 300 K.

We have synthesized polycrystalline $CoFeV_{0.5}Mn_{0.5}Si$ to investigate the effects of the partial substitution of V for Mn on the transport and magnetic properties. Density functional calculations [41] indicate that this material should exhibit nearly half-metallic properties; thus, the substitution alters the band structure from that of a nearly spin gapless semiconductor. The research question is twofold: (i) How does the additional substitutional disorder affect the electric transport? (ii) How does the shift in band structure manifest itself in the electronic and magnetic properties? In the remainder of this paper, we present details of the experiment, the results and their interpretation, and concluding observations.

2. Experimental Methods

2.1 Synthesis and crystal structure

A bulk ingot of $CoFeV_{0.5}Mn_{0.5}Si$ alloy was prepared using arc melting and vacuum annealing. The vacuum annealing was done in a tubular vacuum furnace ($\sim 10^{-7}$ torr) at 600 °C for 24 hours. More details on sample preparation can be found in Ref. [41]. The elemental composition of the annealed sample was determined using energy-dispersive x-ray spectroscopy (EDS). The composition was found to be $Co_{1.00}Fe_{1.00}Mn_{0.51}V_{0.51}Si_{0.98}$, which agrees well with the nominal composition. To understand the crystal structure and possible disorder, we analyzed the powder x-ray diffraction pattern of the annealed sample, which was recorded using a Rigaku MiniFlex600

x-ray diffractometer with a Cu-K_α source (λ = 1.54 Å). Figure 1 shows the room-temperature x-ray diffraction (XRD) pattern of the powder sample of the annealed $CoFeV_{0.5}Mn_{0.5}Si$ alloy, which indicates that the sample is polycrystalline with a cubic Heusler structure. The XRD pattern contains both the fundamental and superlattice peaks expected for the ordered phase. The presence of (111) and (200) superlattice peaks indicates the formation of conventional $L2_1$ or Y-type ordering in Heusler alloys, rather than complete disorder between the atoms (A2-type) or partial atomic disorder (B2-type). Given that the sample is a quaternary Heusler alloy, we started the data analysis with a fully ordered, XX'YZ, (X=Fe, X'=Co, Y=Mn/V and Z = Si), Y-type structure (prototype LiMgPdSn) model and introduced various types of atomic disorder to fit the whole profile using the Rietveld method. The relative intensities, mainly of the (111) and (200) peaks, are very sensitive to the structural disorder. It is difficult to distinguish the site exchange between Co and Fe using Cu K_α radiation; however, there was a noticeable improvement in the fit when some A2-type disorder (X/X' ↔ Z) was introduced in the model. Refinement suggests that there could be site exchange of up to 15 % between Fe/Co and Si. We note that Mn and V are evenly distributed at the Y-site. The lattice parameter obtained from the refinement is a = 5.668 Å.

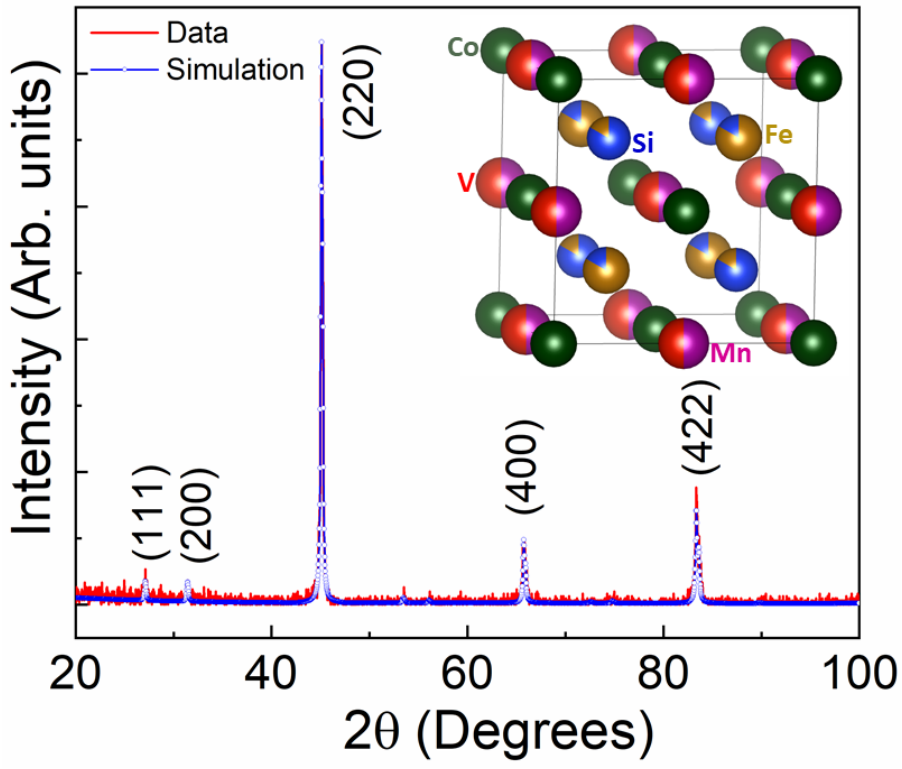

Figure 1: Room temperature x-ray diffraction pattern recorded on $CoFeV_{0.5}Mn_{0.5}Si$ powder sample. The inset shows the partially A2-type disordered cubic crystal structure, where the atoms are color coded.

2.2 Magnetic and transport measurements

Magnetization measurements were performed with a Quantum Design Versalab system and a Quantum Design DynaCool PPMS. To carry out transport measurements, a Hall bar was cut from an ingot with a Buehler diamond saw. The dimensions of the bar were $5.41 \times 2.89 \times 1.75$ mm. EPO-TEK EJ2189-LV silver epoxy was used to attach gold leads to the Hall bar. Resistance and magnetoresistance measurements were performed with the PPMS, using the Electric Transport Option (ETO). The raw measurements were symmetrized to account for a small offset in lead positions.

3. Results and Discussion

3.1 Electronic structure and resistivity

Figure 2 shows calculated total density of states (DOS) of CoFeMnSi (a) and $CoFeV_{0.5}Mn_{0.5}Si$ (b). Both compounds exhibit nearly perfect spin polarization. Here, the spin polarization, *SP* is defined as $SP = (N_{\uparrow}(E_F) - N_{\downarrow}(E_F)) \,/\, (N_{\uparrow}(E_F) + N_{\downarrow}(E_F))$, where $N_{\uparrow\downarrow}(E_F)$ is the spin-dependent density of states at the Fermi level, E_F [42]. The calculated spin polarization values are indicated in the figure. In addition to being half-metallic, CoFeMnSi also exhibits nearly gapless behavior of majority-spin states, consistent with earlier reports [40]. More details on electronic structure calculations of $CoFeV_{0.5}Mn_{0.5}Si$, including a description of computational methods can be found in our recent publication [41].

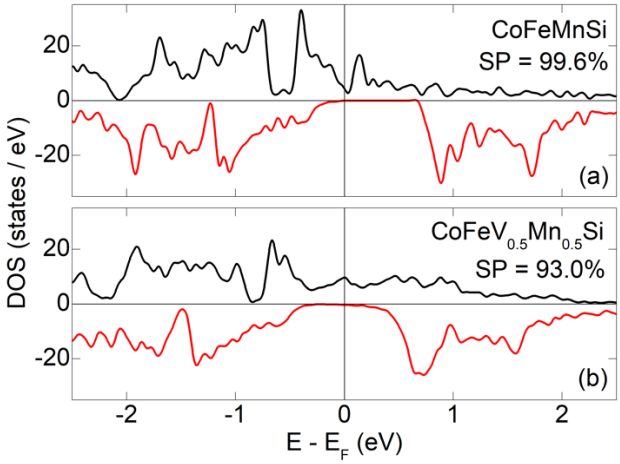

Figure 2. Calculated density of states of CoFeMnSi (a), and $CoFeV_{0.5}Mn_{0.5}Si$ (b). Positive DOS (black line) corresponds to majority-spin, negative DOS (red line) corresponds to minority-spin. Vertical line indicates position of the Fermi level. Calculated spin polarization values are indicated in the figure.

Figure 3 shows the longitudinal resistivity as a function of temperature at zero magnetic field for $CoFeV_{0.5}Mn_{0.5}$ Si. We will first describe the qualitative features of the behavior, which will be followed by a more quantitative discussion. The resistivity as a function of temperature exhibits two main characteristics: (i) there is a minimum in the resistivity at approximately 150 K; and (ii) the change in resistivity between the minimum and the values at the lowest and highest measured temperatures is very small (~1%). It is also noteworthy that the resistivities over the entire temperature range ($5 \leq T \leq 350$ K) are greater than 240 $\mu\Omega \cdot$ cm, which is rather large and characteristic of disordered alloys [28]. These characteristics are all consistent with the Mooij rule [43], an empirical property observed in high-resistivity metallic systems. The Mooij rule can be stated as [44]:

$$\rho_{xx} = \rho_0 + \rho_1(T), \qquad (\rho_1 \ll \rho_0) \tag{1}$$

where

$$\left.\begin{array}{ll} \frac{d\rho_1}{dT} > 0 & \text{if } \rho_0 < \rho_M \\ \frac{d\rho_1}{dT} < 0 & \text{if } \rho_0 > \rho_M. \end{array}\right\} \tag{2}$$

In Eq. (1), ρ_{xx} is the longitudinal resistivity, ρ_0 is the Boltzmann resistivity and ρ_1 is the temperature-dependent correction to the resistivity due to various scattering mechanisms. In Eq. (2), the empirical Mooij resistivity $\rho_M \approx$ 150 $\mu\Omega$cm. As is observed in the $CoFeV_{0.5}Mn_{0.5}Si$ material investigated in this work, metallic systems with $\rho_0 > \rho_M$ often display a minimum in the resistivity, with the temperature coefficient of resistivity being negative at lower temperatures. Howson and Gallagher [45] created a plot demonstrating the Mooij rule for a wide variety of metallic systems. Interestingly, metal-metal binary systems with $\rho_0 > \rho_M$ tended to have relatively small temperature coefficients of resistivity $[\alpha = (1/\rho_{xx})d\rho_{xx}/dT]$ values of ~10^{-4} K^{-1} or less. Metal-metalloid systems showed nearly the opposite behavior, with α values tending to be greater than 10^{-4} K^{-1}. With an average α value of ~10^{-4} K^{-1} (10 – 100 K), the $CoFeV_{0.5}Mn_{0.5}Si$ material we have investigated seems to fittingly interpolate between the two trends.

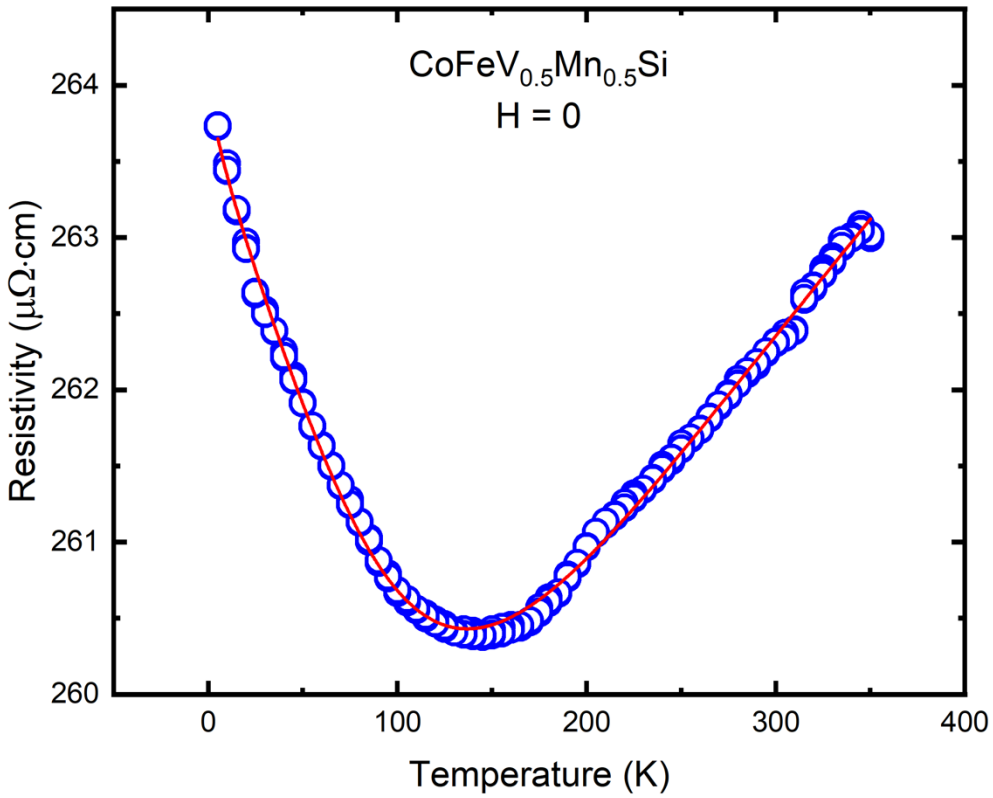

Figure 3: Longitudinal resistivity versus temperature in zero magnetic field for bulk $CoFeV_{0.5}Mn_{0.5}Si$. A minimum occurs at ~150 K. Note that the high-temperature behavior is nearly linear, as would be expected from electron-phonon scattering. The bold line is a fit according to Eq. (3) in the text.

Another noteworthy feature in Howson and Gallagher's plot is the absence of ferromagnetic materials with $\rho_0 > \rho_M$. As one might expect, some ferromagnetic Heusler alloys, with their greater number of atomic constituents (and disordered arrangements in many cases), do possess resistivities high enough to push α into the negative regime. Examples are: Mn_2CoAl [17,46,47], CoFeCrGa [48], and CoFeMnSi [40,49]. All three of these materials are predicted (via density functional theory) to be spin gapless semiconductors. These materials also have monotonically decreasing resistivities with increasing temperature up to room temperature and beyond. Thus, any resistivity minimum would be at even higher temperatures. Heusler alloys that exhibit a resistivity minimum between 5 K and 400 K include $Co_2Mn_xTi_{1-x}Al$ [50] and Co_2FeSi[27,35]. We note that there are also non-Heusler ferromagnetic materials that exhibit a resistivity minimum, e.g., nanowires [25]. Further, the Kondo effect is a widely recognized mechanism leading to a resistivity

minimum and logarithmic temperature dependence at low temperatures. However, the Kondo effect is due to magnetic scattering of conduction electrons from dilute magnetic impurities. The very weak dependence of the resistivity of $CoFeV_{0.5}Mn_{0.5}Si$ on magnetic field makes it unlikely that the Kondo effect is the cause of the resistivity minimum we have observed [51]. Finally, resistivity minima have been observed in Weyl semimetals [52] and double-perovskite oxides [53].

Kaveh and Mott proved theoretically that the Mooij rule is a limited case of a more general principle. Even in systems with relatively low resistivity, there can be a resistivity minimum with the attendant negative temperature coefficient of resistivity if a low enough temperature can be experimentally accessed. The Heusler alloys mentioned above, i.e., Mn_2CoAl, CoFeCrGa, and CoFeMnSi, possess negative temperature coefficients of resistivity for the entire temperature range of the measurements (up to 300 K or 400 K). The resistivities of the bulk materials are all greater than 300 $\mu\Omega$cm; thus, one would expect $CoFeV_{0.5}Mn_{0.5}Si$, with its smaller resistivity, to have a resistivity minimum at a lower temperature, as borne out by our data. We note that the thin-film sample of Mn_2CoAl investigated by Buckley *et al* [47] had a resistivity of ~200 $\mu\Omega$cm at 300 K and yet possessed a negative temperature coefficient of resistivity up to the maximum measurement temperature of 400 K. However, it was also pointed out by Buckley *et al* that Mn_2CoAl films discussed in the literature had a range of room-temperature resistivities and in some cases, non-linear resistance-versus-temperature behavior. They posited that the variety of transport characteristics is likely due to differences in type and extent of anti-site and compositional disorder. It is noteworthy that Hazra *et al* prepared films of Co_2FeSi with different levels of crystalline disorder to study its effects in one alloy system [27,35]. The most disordered films exhibited resistivity minima that shifted to higher temperatures as the level of disorder increased. The films with high levels of crystallinity exhibited no resistivity minima and behaved like standard crystalline metals. Similar trends were seen in thin films of the substitutional disordered alloys $Co_2Mn_xTi_{1-x}Al$ [50] and $Co_2Cr_{1-x}Fe_xAl$ [54].

Theoretical discussions of the negative temperature coefficient of resistivity in high-resistivity metals attribute this behavior to localization induced by quantum interference effects [28,44,55,56]. Weak localization (WL) originates from constructive interference between electron waves multiply scattered along pairs of self-crossing, time-reversed paths, thereby enhancing the probability of backscattering. In general, the strength of localization effects depends on three length scales: the Fermi wavelength ($1/k_F$), the elastic scattering length (l_e), and the inelastic

scattering length (l_{in}) [28,44]. The inelastic scattering length determines the temperature-dependent behavior of the resistivity in the WL regime. Inelastic scattering processes destroy phase coherence and hence diminish localization effects. Thus, if $l_{in} \ll l_e$ (as is the case at high temperatures due to electron-phonon and other types of scattering), weak localization is suppressed. As seen in Fig. 3, the resistivity of $CoFeV_{0.5}Mn_{0.5}Si$ increases nearly linearly with temperature at temperatures above the resistivity minimum, consistent with phonon-dominated scattering at relatively high temperatures. In ferromagnets, $\rho \propto T^2$ behavior is often observed at higher temperatures, which is attributable to electron-magnon scattering [50]. The absence of such behavior in $CoFeV_{0.5}Mn_{0.5}Si$ away from the resistivity minimum suggests that electron-magnon scattering is suppressed, which is consistent with half-metallic behavior [50].

Theory predicts that the temperature-dependent change in conductivity due to weak localization is given by $\Delta\sigma(T) \propto T^{\frac{p}{2}}$, where the parameter p depends on the inelastic scattering process and spatial dimensionality [56]. For example, p = 2 for electron-electron scattering at low temperatures or electron-phonon scattering at high temperatures, whereas p = 3 for electron-phonon scattering at low temperatures. In addition to WL, a resistivity contribution due to enhanced electron-electron Coulomb interaction (EEI) effects is expected to be significant at low temperatures. In this regime, $\Delta\sigma \propto T^{1/2}$ [44,56]. This behavior has been observed in many disordered alloys [26,45]. We therefore fitted our data with an expression indicative of a coexistence of both WL and EEI for temperatures below the resistivity minimum:

$$\rho = \rho_0 - aT^{\frac{1}{2}} - bT^{p/2} + cT^5 \int_0^{\Theta_D/T} \frac{x^5 dx}{(e^x - 1)(1 - e^{-x})}, \qquad (3)$$

where a, b, and c are constants and Θ_D is the Debye temperature. The last term is the Bloch-Grüneisen relation [57]. The fit shown in Fig. 3 has the value of p set at 2 and is very good over the entire range of temperatures. The best fit values are $\rho_0 = 264.07 \pm 0.04\ \mu\Omega$cm, $a = (1.34 \pm 0.14) \times 10^{-7}$, $b = (2.47 \pm 0.11) \times 10^{-8}$, and $c = (4.31 \pm 0.06) \times 10^{-19}$. (The units for the coefficients are not given.) The value of Θ_D was manually varied; its best fit value was 769 K, which is within ~20% of the DFT-calculated value of 629 K for CoFeMnSi (at room temperature) [58]. The best fit without the WL term is markedly worse, suggesting that both

mechanisms are present and significant in determining the low-temperature behavior of $CoFeV_{0.5}Mn_{0.5}Si$. Fitting with $p = 3$ produces a best fit of comparable quality as for $p = 2$; however, the required Debye temperature $\Theta_D = 840$ K, which is much higher than the theoretically predicted value for CoFeMnSi. Clearly, the resistivity minimum observed in $CoFeV_{0.5}Mn_{0.5}Si$ is due to competition between quantum interference effects and inelastic-scattering processes that produce decoherence.

3.2 Magnetoresistance

To gain more insight into the role of localization in the behavior of the resistivity of $CoFeV_{0.5}Mn_{0.5}Si$, we examined the magnetoresistance (MR) of the material. Figure 4 shows the magnetoresistance of $CoFeV_{0.5}Mn_{0.5}Si$ as a function of magnetic field at various fixed temperatures. The field was applied perpendicular to the direction of the current and along the shortest dimension of the Hall bar. There is a small, positive MR at low temperatures, which transitions to a larger, negative MR at higher temperatures (~150 K and above). The MR is approximately linear at the lowest and highest measured temperatures and it does not appear to saturate in a 9-tesla field.

Heusler alloys exhibit a range of MR behaviors. Bulk polycrystalline Mn_2CoAl exhibits similar behavior to $CoFeV_{0.5}Mn_{0.5}Si$, with positive MR at low temperatures and negative MR at high temperatures; however, the MR values are much higher than those for $CoFeV_{0.5}Mn_{0.5}Si$ [17]. In contrast, thin-film Mn_2CoAl exhibits negative MR at all temperatures investigated (4 K – 400 K) [47]. The magnitude of the negative MR is comparable to that of $CoFeV_{0.5}Mn_{0.5}Si$ and is also temperature-dependent. In Ti_2MnAl films, a temperature-dependent switch from positive MR to negative MR similar to that in $CoFeV_{0.5}Mn_{0.5}Si$ and of similar magnitude was observed [59].

Negative MR is characteristic of systems exhibiting WL [28,56]. The reason is that the magnetic flux that threads the closed scattering paths introduces a phase change to the electron paths that is essentially random due to the diffusive nature of the scattering. This dephasing destroys the constructive interference responsible for the increased resistance. In addition, in ferromagnets, negative MR results from spin-disorder scattering that is suppressed by a magnetic field.

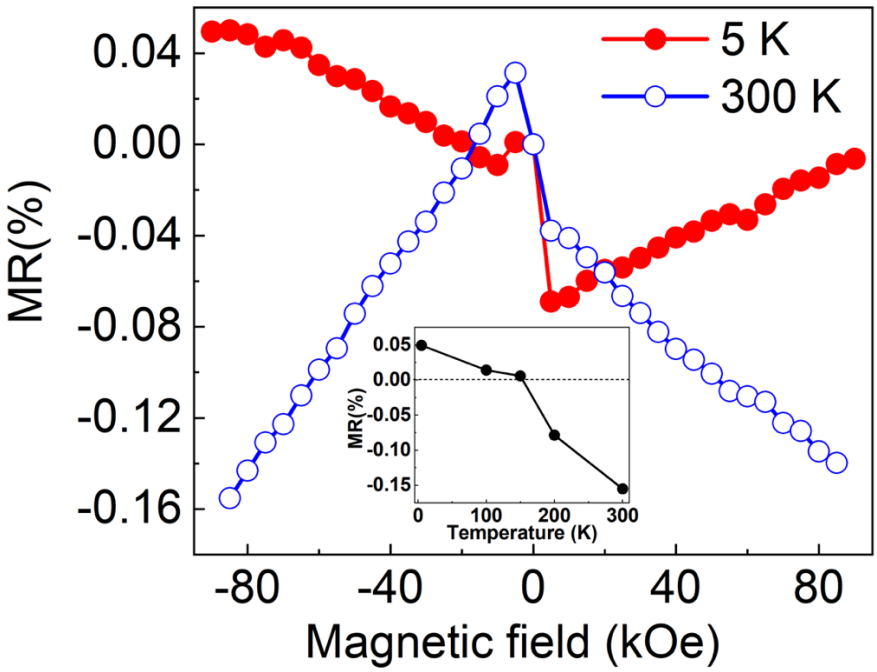

Figure 4: Magnetoresistance ratio versus magnetic field at various temperatures for bulk $CoFeV_{0.5}Mn_{0.5}Si$. The magnetoresistance is positive at low temperatures and negative at high temperatures. The positive/negative field asymmetry likely results from small non-uniformities in the sample (see text). The inset shows the MR ratio at 90 kOe for various temperatures.

A useful illustration of this is the magnetoresistance for a magnetic semiconductor derived from Boltzmann transport theory [60]: $\rho(H)/\rho(0) = \chi_z(H)/\chi_z(0)$, where χ_z is the spin susceptibility along the direction of the magnetic field. It is well known that below the ferromagnetic Curie temperature, χ_z decreases with decreasing temperature and increasing field. Thus, the magnitude of the negative magnetoresistance resulting from spin-disorder scattering increases with increasing temperature.

The spin-orbit interaction has a significant impact on weak localization. Spin-orbit scattering causes a spin-dependent dephasing of the coherent electron loops that leads to a decrease in resistivity. This is weak anti-localization, which results in positive magnetoresistance. However, this mechanism is not operative in ferromagnets, even in the presence of strong spin-orbit interactions [61]. At the same time, linear, positive magnetoresistance has been shown to be a characteristic of the EEI in three dimensions [62]. We therefore conclude that the positive MR at low temperatures is due to EEI, likely in competition with a suppressed negative MR arising from

weak localization because the resistivity increase due to weak localization can be suppressed by the strong internal magnetic field of a ferromagnet [61]. At temperatures higher than the resistivity minimum, we attribute the negative MR to spin-disorder scattering, which becomes dominant at higher temperatures where localization effects are diminished. The coincidence in temperature of the crossover from positive to negative MR and the resistivity minimum is also substantial evidence of the association between positive MR and the EEI.

The small magnitude of the MR of $CoFeV_{0.5}Mn_{0.5}Si$ makes it evident that there is an asymmetry between positive and negative magnetic fields. The anisotropic dip in the resistance at small positive fields is present whether the field variation starts from negative values and ends at positive ones or vice versa. We attribute the asymmetry to a contribution from the transverse resistivity ρ_{xy}; therefore, we discuss this behavior in the next subsection.

3.3 Hall Effect

The transverse (Hall) resistivity ρ_{xy} as a function of magnetic field at different temperatures for $CoFeV_{0.5}Mn_{0.5}Si$ is shown in Fig. 5. The Hall resistivity can be written as

$$\rho_{xy}(B) = R_O B + R_A M, \tag{4}$$

where B is the magnetic induction, R_O is the ordinary Hall coefficient, and R_A is the anomalous Hall coefficient. Comparing Fig. 5 with Fig. 6, which shows the magnetization as a function of magnetic field, it is clear that the anomalous contribution dominates ρ_{xy} in $CoFeV_{0.5}Mn_{0.5}Si$, as it does in other ferromagnets. The carrier density n as a function of temperature was extracted from $R_O(T)$ using a single-band model and is shown in the inset of Fig. 5. The carrier density increases with temperature with a small, approximately linear variation between 4 K and 265 K. Thus, the minimum and subsequent rise in ρ_{xx} at low temperatures is not due to semiconducting behavior and strengthens our conclusion that the minimum in ρ_{xx} is localization-driven. We further note that the relatively weak temperature dependence of n is similar to that of the bulk "parent" material CoFeMnSi, though the values are about 3 orders of magnitude lower than we have found in $CoFeV_{0.5}Mn_{0.5}Si$ [40]. Bulk CoFeMnSi has been identified as a spin gapless semiconductor whereas first-principles calculations indicate half-metallicity in $CoFeV_{0.5}Mn_{0.5}Si$ [41]. A thin-film

sample of CoFeMnSi also exhibited a weak temperature dependence of its carrier density and values that were an order of magnitude lower than those for $CoFeV_{0.5}Mn_{0.5}Si$ [63].

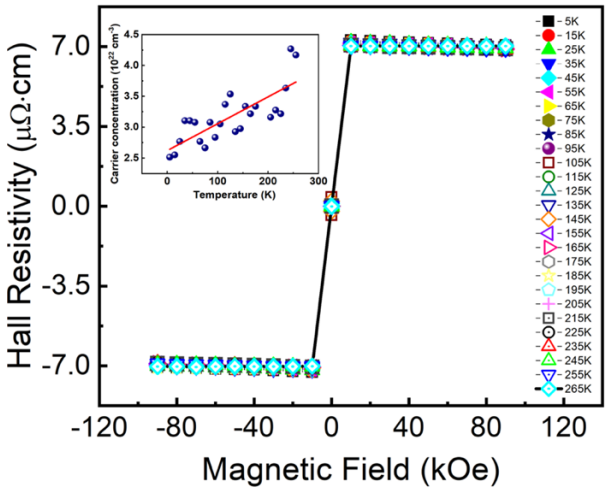

Figure 5: Hall resistivity versus magnetic field at various temperatures for bulk $CoFeMn_{0.5}V_{0.5}Si$. The inset shows the carrier density *n* (extracted from the Hall resistivity) as a function of temperature.

The anomalous Hall resistivity ρ_{xy}^{AHE} was obtained from the *y*-intercept of the linear fit to the ordinary Hall resistivity. As previously mentioned, three mechanisms contribute to ρ_{xy}^{AHE}: (i) an intrinsic band structure-dependent (or Berry curvature-dependent) process; (ii) an extrinsic skew-scattering process; and (iii) an extrinsic side-jump process. The three mechanisms are functions of the longitudinal resistivity. The skew-scattering contribution $\propto \rho_{xx}$ and both the intrinsic and side jump contributions $\propto \rho_{xx}^2$. Skew scattering (linear ρ_{xx} scaling) tends to be dominant in the low-resistivity ("clean limit") regime, while the side jump and/or intrinsic mechanisms (quadratic ρ_{xx} scaling) dominate in higher-resistivity ("dirty metal") systems [34]. (At very high levels of disorder, the simple linear or quadratic scaling behavior breaks down.) Considering both intrinsic and extrinsic mechanisms, ρ_{xy}^{AHE} can be written as

$$\rho_{xy}^{AHE} = a_{sk}\rho_{xx} + a_{sj,i}\rho_{xx}^2, \tag{5}$$

where the coefficients characterize the three mechanisms. (The parameter $a_{sj,i}$ contains contributions from both intrinsic and side jump mechanisms.) ρ_{xx} contains both a temperature-dependent component (ρ_{xxT}) and the residual resistivity (ρ_{xx0}). We must separate these pieces in

order to disentangle the two contributions by fitting the $\rho_{xy}^{AHE}(T)$ data with Eq. (5). Accordingly, Eq. (5) can be rewritten as

$$\rho_{xy}^{AHE} = (a_{sk}\rho_{xx0} + a_{sj,i}\rho_{xx0}^{2}) + (a_{sk} + 2a_{sj,i}\rho_{xx0})\rho_{xxT} + a_{sj,i}\rho_{xxT}^{2}. \qquad (6)$$

Hence, the linear coefficient contains both skew scattering and side jump/intrinsic contributions. The presence of a quadratic dependence is due to the side jump and intrinsic processes. Typically, an extrapolation to zero temperature is done to obtain ρ_{xx0}; however, because of the presence of an upturn in the resistivity at low temperatures due to quantum interference effects, it is advantageous to recast the preceding expressions in terms of the anomalous Hall conductivity.

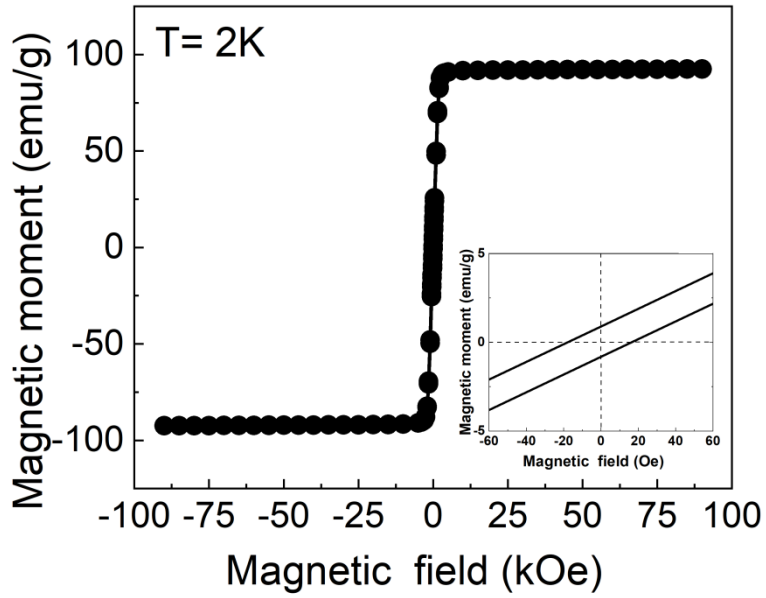

Figure 6: Magnetization versus magnetic field at 2 K for bulk $CoFeV_{0.5}Mn_{0.5}Si$. Note the similarity in behavior between the Hall resistivity and the magnetization, which is a manifestation of the anomalous Hall effect. The inset shows an expanded view of the region around $H = 0$.

The equivalent relationship to Eq. (5) is

$$\sigma_{xy}^{AHE} = b_{sj,i} + b_{sk}\sigma_{xx}. \qquad (7)$$

In this case, the side jump and intrinsic contributions are independent of σ_{xx} and the skew-scattering contribution is linear in σ_{xx}. Separating the temperature dependent and residual components of σ_{xx} gives

$$\sigma_{xy}^{AHE} = (b_{sj,i} + b_{sk}\sigma_{xx0}) + b_{sk}\sigma_{xxT}. \quad (8)$$

The experimental value of σ_{xx0} was obtained by linear extrapolation of σ_{xx} to 0 K. Figure 7 shows a plot of σ_{xy}^{AHE} versus σ_{xxT}, which clearly indicates that σ_{xy}^{AHE} is independent of σ_{xxT} at temperatures up to the resistivity minimum, with a constant value of 115 Scm^{-1}. This represents strong evidence that the intrinsic and/or side jump mechanisms are dominant in the anomalous Hall effect in $CoFeV_{0.5}Mn_{0.5}Si$. We also note that σ_{xy}^{AHE}= 115 Scm^{-1} is somewhat smaller than the 162 Scm^{-1} value found for the "parent" material CoFeMnSi [40]. It is much smaller than the room-temperature values for elemental ferromagnets Fe (1032 Scm^{-1}) [64] and Co (480 Scm^{-1}) [65]. The latter values have been entirely accounted for theoretically by the intrinsic contribution [29,31]. Side-jump contributions tend to be much smaller [65]; thus, they may be significant in $CoFeV_{0.5}Mn_{0.5}Si$ given the low value of σ_{xy}^{AHE}.

Clearly, σ_{xy}^{AHE} is constant over a relatively wide temperature range, but the very weak temperature dependence of σ_{xx} results in a narrow corresponding range for σ_{xx}. Thus, we cannot determinatively compare the σ_{xy}^{AHE} plateau region in $CoFeV_{0.5}Mn_{0.5}Si$ with those of other materials with a much wider range of σ_{xx} values [65]. It is, however, worthwhile to mention that the σ_{xy}^{AHE} plateau region in $CoFeV_{0.5}Mn_{0.5}Si$ occurs at σ_{xx} values that are at least an order of magnitude smaller than in the elemental ferromagnets and several other materials [65]. It is significant that this behavior occurs in the regime where localization dominates the temperature dependence of σ_{xx} , indicating that the scattering mechanisms that contribute to localization in $CoFeV_{0.5}Mn_{0.5}Si$ have negligible impact on the behavior of σ_{xy}^{AHE}.

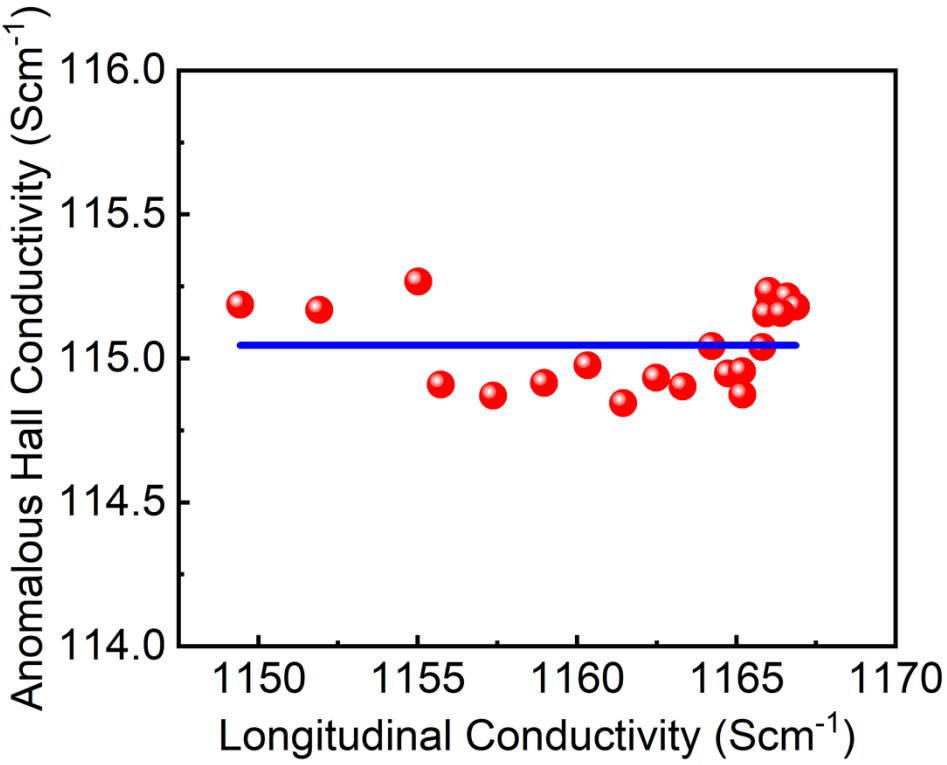

Figure 7: Anomalous Hall conductivity versus longitudinal conductivity for bulk $CoFeV_{0.5}Mn_{0.5}Si$ for temperatures below the longitudinal resistivity minimum. The anomalous Hall conductivity is virtually constant in this temperature regime, indicating the dominance of the intrinsic and/or side-jump mechanisms.

Several theoretical works have addressed the influence of localization on σ_{xy}^{AHE} in disordered magnetic metals, with primary focus on two-dimensional systems [36–38]. Dugaev *et al* [38] show that the weak-localization correction to the side-jump contribution to $\sigma_{xy}^{AHE}$is negligible in three dimensions (and, in fact, for any number of dimensions). The localization correction to the skew-scattering contribution, is however, non-zero. The absence of EEI effects on the behavior of σ_{xy}^{AHE} in two dimensions has been rigorously established [37]. More recently, Li and Levchenko obtained the temperature dependence of the quantum correction to σ_{xy}^{AHE} due to EEI in three dimensions [66]. They show that $\delta\sigma_{xy}^{AHE} \propto \sqrt{T}ln^{-1}(T_0/T)$ for both side jump and skew scattering contributions for disordered metallic systems that are not spin polarized. For ferromagnetic systems, they find that for temperatures below the exchange splitting, the skew scattering contribution should be further suppressed. We also note that Yang *et al.* show that the side jump contribution depends strongly on the spin structure of the scattering potential and in particular, magnon scattering contributes to the side jump component [67]. Thus, in materials such as $CoFeV_{0.5}Mn_{0.5}Si$ in which

the transport current is significantly spin polarized, the attendant reduction of single-magnon scattering may suppress the side jump component relative to the skew scattering contribution. Thus, it is plausible that in a 3D ferromagnet with spin-polarized transport, corrections to σ_{xy}^{AHE} due to both weak localization and EEI may be suppressed, in accord with our experimental results. Further, if the reduction in magnon scattering suppresses the side jump mechanism in general, the intrinsic mechanism may therefore be dominant in the anomalous Hall effect in $CoFeV_{0.5}Mn_{0.5}Si$.

Finally, we go back to the asymmetry in the magnetoresistance. We note that MR anomalies close to zero field were also seen in Mn_2CoAl films [47] and bulk polycrystalline Mn_2CoAl [17]. In the latter case, a significant asymmetry between positive and negative fields was also obtained. Typically, small-field anomalies are explained in terms of the multi-domain magnetization state of the sample near zero field [59]. As seen in Fig. 4, however, the asymmetry persists even at large field magnitudes. There is also generally a difference in the slopes of the $\rho(H)$ data for positive and negative fields. MR asymmetry is usually linked to magnetization reversal [68]; however, the coercivity of $CoFeV_{0.5}Mn_{0.5}Si$ is very small (~20 Oe) and there is no dip on the negative side of zero field (Fig. 6). Thus, it seems unlikely that the asymmetry that persists at high fields results from hysteretic switches in the magnetization.

A more probable source of the asymmetry lies in non-uniformity in the transverse voltage along the sample. Such a non-uniformity e.g., due to changes in thickness across the sample, can lead to mixing of off-diagonal resistivity components with the longitudinal resistivity [69,70]. The mixing of the anomalous Hall effect produces a contribution to ρ_{xx} that is odd in the magnetic field and would lead to the observed asymmetry in the magnetoresistance. The symmetric (intrinsic) magnetoresistance is very small; thus, the asymmetry is significant even though the non-uniformity and resulting mixed-in transverse component may be tiny.

4. Conclusions

We have carried out a comprehensive experimental investigation of the transport and magnetotransport properties of bulk $CoFeV_{0.5}Mn_{0.5}Si$. The partial substitution of V for Mn results in a longitudinal resistivity minimum at ~150 K, whereas no minimum exists between 5 K and 300 K for the "parent" material CoFeMnSi. Further, $CoFeMn_{0.5}V_{0.5}Si$, which DFT calculations indicate is nearly a half-metal, exhibits lower resistivity than CoFeMnSi—a nearly spin gapless semiconductor. The resistivity minimum in $CoFeV_{0.5}Mn_{0.5}Si$ is due to competition between weak

localization (WL) and enhanced electron-electron Coulomb interactions (EEI) at low temperatures and coherence-disrupting inelastic scattering mechanisms at high temperatures. Our results indicate that single-magnon scattering is not a significant contributor to inelastic scattering at higher temperatures, which is consistent with the half-metallicity of $CoFeV_{0.5}Mn_{0.5}Si$. The magnetoresistance exhibits small positive values at low temperatures and small negative values at higher temperatures. The positive magnetoresistance at low temperatures accords with the presence of EEI in the electron transport. Hall measurements give a carrier density that is at least an order of magnitude higher than in CoFeMnSi. The anomalous Hall conductivity has a relatively low value of 115 Scm^{-1} and is independent of the longitudinal conductivity for temperatures up to the resistivity minimum. This indicates that the intrinsic and/or side-jump mechanisms are the dominant contributors. It is significant that the scattering independence of the anomalous Hall conductivity is operative in the same temperature regime where WL and EEI are dominant. Hence, the quantum corrections to resistivity do not affect the behavior of the anomalous Hall conductivity in the $CoFeV_{0.5}Mn_{0.5}Si$ 3D ferromagnetic system. Further experimental and theoretical work to illuminate the evolution of the band structure (and hence the intrinsic contribution to the anomalous Hall conductivity) of $CoFeMn_{1-x}V_xSi$ with varying vanadium content is very much desirable.

Acknowledgements

We gratefully acknowledge the support received from the National Science Foundation under grant nos. DMR 2003828 and DMR 2003856. These grants were awarded under the auspices of the EPSCoR program.

References

[1] P.J. Webster, *Heusler alloys*, Contemp. Phys. 10 (1969) 559–577. https://doi.org/10.1080/00107516908204800.

[2] P.J. Webster, *Magnetic and chemical order in Heusler alloys containing cobalt and manganese*, J. Phys. Chem. Solids. 32 (1971) 1221–1231. https://doi.org/10.1016/S0022-3697(71)80180-4.

[3] J. Kübler, A.R. William, C.B. Sommers, *Formation and coupling of magnetic moments in Heusler alloys*, Phys. Rev. B. 28 (1983) 1745. https://doi.org/10.1103/PhysRevB.28.1745.

[4] C. Felser, L. Wollmann, S. Chadov, G.H. Fecher, S.S. Parkin, *Basics and prospective of magnetic Heusler compounds,* APL Mater. 3 (2015) 041518. https://doi.org/10.1063/1.4917387.

[5] T. Graf, S.S. Parkin, C. Felser, *Heusler compounds—A material class with exceptional properties*, IEEE Trans. Magn. 47 (2010) 367–373. https://doi.org/10.1109/TMAG.2010.2096229.
[6] L. Bainsla, K.G. Suresh, *Equiatomic quaternary Heusler alloys: A material perspective for spintronic applications*, Appl. Phys. Rev. 3 (2016) 031101. https://doi.org/10.1063/1.4959093.
[7] R.A. De Groot, F.M. Mueller, P.G. Van Engen, K.H.J. Buschow, *New class of materials: half-metallic ferromagnets*, Phys. Rev. Lett. 50 (1983) 2024. https://doi.org/10.1103/PhysRevLett.50.2024.
[8] V.Y. Irkhin, M.I. Katsnel'son, *Half-metallic ferromagnets*, Phys.-Uspekhi. 37 (1994) 659. https://doi.org/10.1070/PU1994v037n07ABEH000033.
[9] M.I. Katsnelson, V.Y. Irkhin, L. Chioncel, A.I. Lichtenstein, R.A. de Groot, *Half-metallic ferromagnets: From band structure to many-body effects*, Rev. Mod. Phys. 80 (2008) 315. https://doi.org/10.1103/RevModPhys.80.315.
[10] W.E. Pickett, J.S. Moodera, *Half metallic magnets*, Phys. Today. 54 (2001) 39–45. https://doi.org/10.1063/1.1381101.
[11] J.M.D. Coey, M. Venkatesan, *Half-metallic ferromagnetism: Example of CrO_2*, J. Appl. Phys. 91 (2002) 8345–8350. https://doi.org/10.1063/1.1447879.
[12] D.D. Awschalom, M.E. Flatté, *Challenges for semiconductor spintronics*, Nat. Phys. 3 (2007) 153–159. https://doi.org/10.1038/nphys551.
[13] A. Hirohata, K. Yamada, Y. Nakatani, I.-L. Prejbeanu, B. Diény, P. Pirro, B. Hillebrands, Review on spintronics: Principles and device applications, J. Magn. Magn. Mater. 509 (2020) 166711. https://doi.org/10.1016/j.jmmm.2020.166711.
[14] S.D. Bader, S.S.P. Parkin, *Spintronics*, Annu Rev Condens Matter Phys. 1 (2010) 71–88. https://doi.org/10.1146/annurev-conmatphys-070909-104123.
[15] I. Žutić, J. Fabian, S. Das Sarma, *Spintronics: Fundamentals and applications*, Rev. Mod. Phys. 76 (2004) 323. https://doi.org/10.1103/RevModPhys.76.323.
[16] Z. Yue, Z. Li, L. Sang, X. Wang, *Spin-Gapless Semiconductors*, Small. 16 (2020) 1905155. https://doi.org/10.1002/smll.201905155.
[17] S. Ouardi, G.H. Fecher, C. Felser, J. Kübler, *Realization of spin gapless semiconductors: The Heusler compound Mn_2CoAl*, Phys. Rev. Lett. 110 (2013) 100401. https://doi.org/10.1103/PhysRevLett.110.100401.
[18] P. Lukashev, P. Kharel, S. Gilbert, B. Staten, N. Hurley, R. Fuglsby, Y. Huh, S. Valloppilly, W. Zhang, K. Yang, R. Skomski, D.J. Sellmyer, *Investigation of spin-gapless semiconductivity and half-metallicity in Ti_2MnAl-based compounds*, Appl. Phys. Lett. 108 (2016) 141901. https://doi.org/10.1063/1.4945600.
[19] V.V. Marchenkov, V.Y. Irkhin, Half-Metallic Ferromagnets, *Spin Gapless Semiconductors, and Topological Semimetals Based on Heusler Alloys: Theory and Experiment*, Phys. Met. Metallogr. 122 (2021) 1133–1157. https://doi.org/10.1134/S0031918X21120061.
[20] I. Galanakis, P.H. Dederichs, N. Papanikolaou, *Slater-Pauling behavior and origin of the half-metallicity of the full-Heusler alloys*, Phys. Rev. B. 66 (2002) 174429. https://doi.org/10.1103/PhysRevB.66.174429.
[21] I. Galanakis, P. Mavropoulos, P.H. Dederichs, *Electronic structure and Slater–Pauling behaviour in half-metallic Heusler alloys calculated from first principles*, J. Phys. Appl. Phys. 39 (2006) 765. https://doi.org/10.1088/0022-3727/39/5/S01.

[22] S. Skaftouros, K. Özdoğan, E. Şaşıoğlu, I. Galanakis, *Generalized Slater-Pauling rule for the inverse Heusler compounds*, Phys. Rev. B. 87 (2013) 024420. https://doi.org/10.1103/PhysRevB.87.024420.
[23] P.V. Lukashev, Z. Lehmann, L. Stuelke, R. Filippone, B. Dahal, S. Valloppilly, J. Waybright, A.K. Pathak, Y. Huh, P.M. Shand, P. Kharel, *Effect of atomic disorder on electronic, magnetic and electron-transport properties of Ti_2MnAl*, J. Alloys Compd. 895 (2022) 162625. https://doi.org/10.1016/j.jallcom.2021.162625.
[24] P.J. Webster, K.R.A. Ziebeck, *Magnetic and chemical order in Heusler alloys containing cobalt and titanium*, J. Phys. Chem. Solids. 34 (1973) 1647–1654. https://doi.org/10.1016/S0022-3697(73)80130-1.
[25] M. Brands, A. Carl, O. Posth, G. Dumpich, *Electron-electron interaction in carbon-coated ferromagnetic nanowires*, Phys. Rev. B. 72 (2005) 085457. https://doi.org/10.1103/PhysRevB.72.085457.
[26] D. Biswas, A.K. Meikap, S.K. Chattopadhyay, S.K. Chatterjee, J.-J. Lin, *Weak localization and electron–electron interaction in disordered $V_{80}Al_{20}-$* xFex alloys at low temperature, Phys. Lett. A. 328 (2004) 380–386. https://doi.org/10.1016/j.physleta.2004.06.016.
[27] B.K. Hazra, S.N. Kaul, S. Srinath, M.M. Raja, R. Rawat, A. Lakhani, *Diffuson contribution to anomalous Hall effect in disordered Co_2FeSi thin films*, J. Magn. Magn. Mater. 481 (2019) 194–202. https://doi.org/10.1016/j.jmmm.2019.02.081.
[28] J.S. Dugdale, *The electrical properties of disordered metals*, Cambridge University Press, 1995.
[29] Y. Yao, L. Kleinman, A.H. MacDonald, J. Sinova, T. Jungwirth, D. Wang, E. Wang, Q. Niu, *First principles calculation of anomalous Hall conductivity in ferromagnetic bcc Fe*, Phys. Rev. Lett. 92 (2004) 037204. https://doi.org/10.1103/PhysRevLett.92.037204.
[30] K. Manna, L. Muechler, T.-H. Kao, R. Stinshoff, Y. Zhang, J. Gooth, N. Kumar, G. Kreiner, K. Koepernik, R. Car, J. Kübler, G.H. Fecher, C. Shekhar, Y. Sun, C. Felser, *From colossal to zero: controlling the anomalous Hall effect in magnetic Heusler compounds via Berry curvature design*, Phys. Rev. X. 8 (2018) 041045. https://doi.org/10.1103/PhysRevX.8.041045.
[31] X. Wang, D. Vanderbilt, J.R. Yates, I. Souza, *Fermi-surface calculation of the anomalous Hall conductivity*, Phys. Rev. B. 76 (2007) 195109. https://doi.org/10.1103/PhysRevB.76.195109.
[32] G. Gurung, D.-F. Shao, T.R. Paudel, E.Y. Tsymbal, *Anomalous Hall conductivity of noncollinear magnetic antiperovskites*, Phys. Rev. Mater. 3 (2019) 044409. https://doi.org/10.1103/PhysRevMaterials.3.044409.
[33] S. Onoda, N. Sugimoto, N. Nagaosa, *Intrinsic versus extrinsic anomalous Hall effect in ferromagnets*, Phys. Rev. Lett. 97 (2006) 126602. https://doi.org/10.1103/PhysRevLett.97.126602.
[34] N. Nagaosa, J. Sinova, S. Onoda, A.H. MacDonald, N.P. Ong, *Anomalous Hall effect*, Rev. Mod. Phys. 82 (2010) 1539. https://doi.org/10.1103/RevModPhys.82.1539.
[35] B.K. Hazra, S.N. Kaul, S. Srinath, M.M. Raja, R. Rawat, A. Lakhani, *Evidence for the absence of electron-electron coulomb interaction quantum correction to the anomalous Hall effect in Co_2FeSi Heusler-alloy thin films*, Phys. Rev. B. 96 (2017) 184434. https://doi.org/10.1103/PhysRevB.96.184434.
[36] A. Langenfeld, P. Wölfle, *Absence of quantum corrections to the anomalous Hall conductivity*, Phys. Rev. Lett. 67 (1991) 739. https://doi.org/10.1103/PhysRevLett.67.739.

[37] K.A. Muttalib, P. Wölfle, *Disorder and temperature dependence of the anomalous Hall effect in thin ferromagnetic films: Microscopic model*, Phys. Rev. B. 76 (2007) 214415. https://doi.org/10.1103/PhysRevB.76.214415.
[38] V.K. Dugaev, A. Crépieux, P. Bruno, *Localization corrections to the anomalous Hall effect in a ferromagnet*, Phys. Rev. B. 64 (2001) 104411. https://doi.org/10.1103/PhysRevB.64.104411.
[39] P. Mitra, N. Kumar, N. Samarth, *Localization and the anomalous Hall effect in a dirty metallic ferromagnet*, Phys. Rev. B. 82 (2010) 035205. https://doi.org/10.1103/PhysRevB.82.035205.
[40] L. Bainsla, A.I. Mallick, M.M. Raja, A.K. Nigam, B.C.S. Varaprasad, Y.K. Takahashi, A. Alam, K.G. Suresh, K. Hono, *Spin gapless semiconducting behavior in equiatomic quaternary CoFeMnSi Heusler alloy*, Phys. Rev. B. 91 (2015) 104408. https://doi.org/10.1103/PhysRevB.91.104408.
[41] P. Kharel, G. Baker, M. Flesche, A. Ramker, Y. Moua, S. Valloppilly, P.M. Shand, P.V. Lukashev, *Electronic band structure and magnetism of $CoFeV_{0.5}Mn_{0.5}Si$*, AIP Adv. 12 (2022) 035011. https://doi.org/10.1063/9.0000252.
[42] J.P. Velev, P.A. Dowben, E.Y. Tsymbal, S.J. Jenkins, A.N. Caruso, *Interface effects in spin-polarized metal/insulator layered structures*, Surf. Sci. Rep. 63 (2008) 400–425. https://doi.org/10.1016/j.surfrep.2008.06.002.
[43] J.H. Mooij, *Electrical conduction in concentrated disordered transition metal alloys*, Phys. Status Solidi A. 17 (1973) 521–530. https://doi.org/10.1002/pssa.2210170217.
[44] M. Kaveh, N.F. Mott, *Universal dependences of the conductivity of metallic disordered systems on temperature, magnetic field and frequency*, J. Phys. C Solid State Phys. 15 (1982) L707. https://doi.org/10.1088/0022-3719/15/22/004.
[45] M.A. Howson, B.L. Gallagher, *The electron transport properties of metallic glasses*, Phys. Rep. 170 (1988) 265–324. https://doi.org/10.1016/0370-1573(88)90145-7.
[46] S. Ouardi, G.H. Fecher, C. Felser, J. Kübler, *Erratum: Realization of Spin Gapless Semiconductors: The Heusler Compound Mn_2CoAl* [Phys. Rev. Lett. 110, 100401 (2013)], Phys. Rev. Lett. 122 (2019) 059901. https://doi.org/10.1103/PhysRevLett.122.059901.
[47] R.G. Buckley, T. Butler, C. Pot, N.M. Strickland, S. Granville, *Exploring disorder in the spin gapless semiconductor Mn_2CoAl*, Mater. Res. Express. 6 (2019) 106113. https://doi.org/10.1088/2053-1591/ab3bd3.
[48] L. Bainsla, A.I. Mallick, M.M. Raja, A.A. Coelho, A.K. Nigam, D.D. Johnson, A. Alam, K.G. Suresh, *Origin of spin gapless semiconductor behavior in CoFeCrGa*: Theory and Experiment, Phys. Rev. B. 92 (2015) 045201. https://doi.org/10.1103/PhysRevB.92.045201.
[49] L. Bainsla, R. Yilgin, J. Okabayashi, A. Ono, K. Suzuki, S. Mizukami, *Structural and magnetic properties of epitaxial thin films of the equiatomic quaternary CoFeMnSi Heusler alloy*, Phys. Rev. B. 96 (2017) 094404. https://doi.org/10.1103/PhysRevB.96.094404.
[50] M. Aftab, G.H. Jaffari, S.K. Hasanain, T.A. Abbas, S.I. Shah, *Disorder and weak localization effects in $Co_2Mn_xTi_{1-x}Al$ Heusler alloy thin films*, J. Phys. Appl. Phys. 45 (2012) 475001. https://doi.org/10.1088/0022-3727/45/47/475001.
[51] H.T. He, C.L. Yang, W.K. Ge, J.N. Wang, X. Dai, Y.Q. Wang, *Resistivity minima and Kondo effect in ferromagnetic GaMnAs films*, Appl. Phys. Lett. 87 (2005) 162506. https://doi.org/10.1063/1.2108131.

[52] M. Einaga, K. Shimizu, J. Hu, Z.Q. Mao, A. Politano, *Resistivity of Weyl semimetals NbP and TaP under pressure,* Phys. Status Solidi RRL–Rapid Res. Lett. 11 (2017) 1700182. https://doi.org/10.1002/pssr.201700182.
[53] Z.-C. Wang, L. Chen, S.-S. Li, J.-S. Ying, F. Tang, G.-Y. Gao, Y. Fang, W. Zhao, D. Cortie, X. Wang, *Giant linear magnetoresistance in half-metallic Sr_2CrMoO_6 thin films*, Npj Quantum Mater. 6 (2021) 1–8. https://doi.org/10.1038/s41535-021-00354-1.
[54] R. Kelekar, B.M. Clemens, *Epitaxial growth of the Heusler alloy $Co_2Cr_{1-x}Fe_xAl$*, J. Appl. Phys. 96 (2004) 540–543. https://doi.org/10.1063/1.1759399.
[55] G. Bergmann, *Weak localization in thin films: a time-of-flight experiment with conduction electrons*, Phys. Rep. 107 (1984) 1–58. https://doi.org/10.1016/0370-1573(84)90103-0.
[56] P.A. Lee, T.V. Ramakrishnan, *Disordered electronic systems*, Rev. Mod. Phys. 57 (1985) 287. https://doi.org/10.1103/RevModPhys.57.287.
[57] F.J. Blatt, *Physics of electronic conduction in solids*, McGraw-Hill, 1968.
[58] X. Tan, J. You, P.-F. Liu, Y. Wang, *Theoretical study of the electronic, magnetic, mechanical and thermodynamic properties of the spin gapless semiconductor CoFeMnSi, Crystals*. 9 (2019) 678. https://doi.org/10.3390/cryst9120678.
[59] W. Feng, X. Fu, C. Wan, Z. Yuan, X. Han, N.V. Quang, S. Cho, *Spin gapless semiconductor like Ti_2MnAl film as a new candidate for spintronics application*, Phys. Status Solidi RRL–Rapid Res. Lett. 9 (2015) 641–645. https://doi.org/10.1002/pssr.201510340.
[60] C. Haas, *Spin-disorder scattering and magnetoresistance of magnetic semiconductors*, Phys. Rev. 168 (1968) 531. https://doi.org/10.1103/PhysRev.168.531.
[61] V.K. Dugaev, P. Bruno, J. Barnaś, *Weak localization in ferromagnets with spin-orbit interaction*, Phys. Rev. B. 64 (2001) 144423. https://doi.org/10.1103/PhysRevB.64.144423.
[62] A. Gerber, I. Kishon, I.Y. Korenblit, O. Riss, A. Segal, M. Karpovski, B. Raquet, *Linear positive magnetoresistance and quantum interference in ferromagnetic metals*, Phys. Rev. Lett. 99 (2007) 027201. https://doi.org/10.1103/PhysRevLett.99.027201.
[63] V. Mishra, V. Barwal, L. Pandey, N.K. Gupta, S. Hait, A. Kumar, N. Sharma, N. Kumar, S. Chaudhary, *Investigation of spin gapless semiconducting behaviour in quaternary CoFeMnSi Heusler alloy thin films on Si (1 0 0)*, J. Magn. Magn. Mater. 547 (2022) 168837. https://doi.org/10.1016/j.jmmm.2021.168837.
[64] P.N. Dheer, *Galvanomagnetic effects in iron whiskers*, Phys. Rev. 156 (1967) 637. https://doi.org/10.1103/PhysRev.156.637.
[65] T. Miyasato, N. Abe, T. Fujii, A. Asamitsu, S. Onoda, Y. Onose, N. Nagaosa, Y. Tokura, *Crossover behavior of the anomalous Hall effect and anomalous Nernst effect in itinerant ferromagnets*, Phys. Rev. Lett. 99 (2007) 086602. https://doi.org/10.1103/PhysRevLett.99.086602.
[66] S. Li, A. Levchenko, *Temperature Dependence of the Anomalous Hall Effect from Electron Interactions*, Phys. Rev. Lett. 124 (2020) 156802. https://doi.org/10.1103/PhysRevLett.124.156802.
[67] S.A. Yang, H. Pan, Y. Yao, Q. Niu, *Scattering universality classes of side jump in the anomalous Hall effect*, Phys. Rev. B. 83 (2011) 125122. https://doi.org/10.1103/PhysRevB.83.125122.
[68] S. Sahoo, S. Polisetty, Y. Wang, T. Mukherjee, X. He, S.S. Jaswal, C. Binek, *Asymmetric magnetoresistance in an exchange bias Co/CoO bilayer*, J. Phys. Condens. Matter. 24 (2012) 096002. https://doi.org/10.1088/0953-8984/24/9/096002.

[69] A. Segal, O. Shaya, M. Karpovski, A. Gerber, *Asymmetric field dependence of magnetoresistance in magnetic films*, Phys. Rev. B. 79 (2009) 144434. https://doi.org/10.1103/PhysRevB.79.144434.
[70] V.Y. Tkachuk, I.V. Ovsiyenko, L.Y. Matzui, T.A. Len, Y.I. Prylutskyy, O.A. Brusylovets, I.B. Berkutov, I.G. Mirzoiev, O.I. Prokopov, *Asymmetric magnetoresistance in the graphite intercalation compounds with cobalt*, Mol. Cryst. Liq. Cryst. 639 (2016) 137–150. https://doi.org/10.1080/15421406.2016.1255069.